Analytical Methods

ROYAL SOCIETY OF CHEMISTRY

PAPER

View Article Online
View Journal | View Issue

Cite this: *Anal. Methods*, 2024, **16**, 4381

A salivary urea sensor based on a microsieve disposable gate AlGaN/GaN high electron mobility transistor

Guo Yang, [ab] Boxuan Xu,[bc] Hui Chang,[bd] Zhiqi Gu *[b] and Jiadong Li *[ab]

The abundant bio-markers in saliva provide a new option for non-invasive testing. However, due to the presence of impurities in the saliva background, most of the existing saliva testing methods rely on pre-processing, which limits the application of saliva testing as a convenient means of testing in daily life. Herein, a disposable-gate AlGaN/GaN high electron mobility transistor (HEMT) biosensor integrated with a micro-sieve was introduced to solve the problem of signal interference caused by charged impurities in saliva for HEMT based biosensors, where the micro-sieve was utilized as a pre-treatment unit to remove large particles of impurities from saliva through the size effect and thus greatly improving the accuracy of detection. The experimental results showed that the HEMT based biosensor has excellent linearity (R^2 = 0.9977) and a high sensitivity of 6.552 μA dec^{-1} for urea sensing from 1 fM to 100 mM in 0.1× PBS solution. When it comes to artificial saliva detection, compared to the HEMT sensor without the micro-sieve (sensitivity = 3.07432 μA dec^{-1}), the sensitivity of the HEMT sensor integrated with the micro-sieve showed almost no change. Moreover, to verify that urea can be detected in actual saliva, urea is sensed directly in human saliva. The addition of the microsieve module provides a new way for biosensors to detect specific markers in saliva in real time, and the designed HEMT biosensor with the microsieve function has a wide range of application potential in rapid saliva detection.

Received 28th March 2024
Accepted 24th May 2024

DOI: 10.1039/d4ay00551a

rsc.li/methods

1. Introduction

With the rapid advancement of sensing technology, analysis of human exocrine fluid is being considered as a promising non-invasive alternative to blood analysis.[1] Saliva is a complex mixture of liquids comprising mainly protein, urea, uric acid, microorganisms, enzymes and various electrolytes.[2] It is one of the most easily accessible exocrine fluids for humans with healthy individuals producing 1–1.5 L per day through their salivary glands.[3] Studies have shown that levels of certain markers in saliva are significantly correlated with levels of the corresponding markers in the blood.[4–11] Studies have demonstrated significant correlation between certain markers in saliva and corresponding markers in blood; thus saliva can be regarded as "extracellular blood" that can reflect the physiological state of the body without invasive methods.[12–15]

Urea (ure) is produced when proteins break down in mammals' bodies.[16] Recent research has shown that measuring levels of urea in saliva can be used as an effective way to diagnose various illnesses such as kidney problems,[10,17,18] lung disease,[19–21] infections,[22,23] diabetes mellitus,[11,24,25] cancer,[26] hypertension,[25,27] and others. The current method for detecting salivary urea involves using absorption spectrometers.[28] The authors Wang *et al.*[10] presented OFUS (fiber-optic urea sensing), a cost-effective and user-friendly real-time detection system, designed for the precise identification of urea levels in saliva. This system works by breaking down urea into ammonia which then causes a color change in a pH indicator. On another note, Alev-Tuzuner *et al.*[29] used polyethylene glycol (PEG)-based hydrogels with immobilized enzymes called ureases. They applied these hydrogels onto pH paper creating distinct bands. The primary focus of biosensor research is to enhance sensor sensitivity or reduce costs. However, the majority of these endeavors solely concentrate on enhancing the sensor's performance. The potential presence of protein, bacteria, cells, and low urea levels in saliva can result in inaccurate test outcomes and ultimately lead to misdiagnosis, which is often overlooked. Additionally, false results may arise from possible bleeding gums as well as remnants of food and beverages in the oral cavity.[5] To address these challenges effectively, it would be beneficial to consider a method inspired by blood sample processing that utilizes centrifugation (CF) for eliminating cells,

[a]*School of Mechanical and Electrical Engineering, Changchun University of Science and Technology, Changchun, Jilin, 130022, People's Republic of China*
[b]*Key Laboratory of Multifunctional Nanomaterials and Smart Systems, Suzhou Institute of Nano-Tech and Nano-Bionics, Chinese Academy of Sciences, Suzhou 215125, People's Republic of China. E-mail: jdli2009@sinano.ac.cn; zqgu2017@sinano.ac.cn; Tel: +86-512-62872678*
[c]*The College of Materials Science and Engineering, Shanghai University, Shanghai, 200072, People's Republic of China*
[d]*School of Nano Technology and Nano Bionics, University of Science and Technology of China, Hefei, 230026, People's Republic of China*

bacteria, and macromolecules with the aim of improving measurement accuracy. However, in order to implement this method, it is necessary to have centrifugal equipment, which unfortunately hinders the portability of urea sensing systems. Moreover, the cost of centrifugal equipment is usually higher, making it impractical for everyday use. Hence, there is an urgent requirement for a cost-effective and uncomplicated solution to purify intricate saliva samples along with a highly sensitive sensor for swift detection.

FET biosensors, which are based on field-effect transistors, are widely recognized for their distinct advantages such as their ability to be miniaturized and integrated into systems, convenient signal detection, and label-free operation.[30,31] Among FET-based biosensors, the AlGaN/GaN high electron mobility transistor (HEMT) is particularly favored for biosensing due to its non-toxic nature, compatibility with biological systems, and stability in various chemical environments.[32–36] The exceptional responsiveness of the highly sensitive two-dimensional electron gas (2DEG), located near the surface of the AlGaN/GaN HEMT sensor, enables effective detection of changes in surface potential.[37–45] Recent applications have successfully demonstrated the use of AlGaN/GaN HEMT sensors in detecting proteins (biomarkers/antigens),[37,42] ions,[43,44,46] DNA hybridization events,[47,48] and pH levels[38,40,45] within solution or serum samples. However, a challenge remains in directly and rapidly detecting biomolecules in complex physiological solutions like saliva or blood. This difficulty primarily arises from time-consuming centrifugation processes, dilution operations, and bulky testing equipment that hinder the development of specialized AlGaN/GaN HEMT biosensors designed specifically for use with physiological solutions. Therefore, it is crucially important to find a cost-effective and straightforward solution that can purify intricate saliva samples while enabling rapid detection using AlGaN/GaN HEMT biosensors.

In this study, we propose a microsieve module-based AlGaN/GaN HEMT sensor for the direct detection of urea in saliva, as illustrated in Fig. 1. Additionally, we employ a straightforward surface modification and specific binding technique, where one end of the urease enzyme is immobilized onto the disposable grid detection surface of the sensor while the other end is attached to urea to initiate an enzymatic reaction. The interaction between urea and urease induces a change in the surface potential of the disposable gate, enabling precise measurement of urea levels by regulating the channel carrier concentration of the AlGaN/GaN HEMT. Our sensor demonstrated excellent linearity (R^2 = 0.98986) in detecting urea in artificial saliva, exhibiting high sensitivity to urea concentrations ranging from 1 mM to 10 M with a sensitivity of approximately 5.20229 μA dec^{-1}, effectively covering the required range for saliva detection. The design of our disposable gate HEMT device efficiently isolates the sensing area from the operating area, minimizing damage caused by repeated biological functionalization and enhancing the device's aspect ratio and active sensing area. In a 0.1× PBS solution, our sensor can achieve an impressive low detection limit of 1 fM and a wide detection range spanning from 1 fM to 100 mM. These findings underscore the significant potential of utilizing microsieve-based AlGaN/GaN HEMT urea sensors for *in vitro* analysis applications while introducing an innovative approach for saliva analysis.

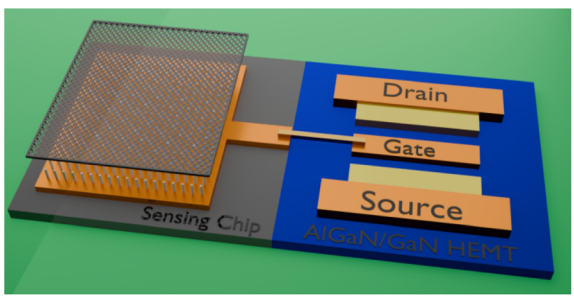

Fig. 1 Three-dimensional model of the disposable gate AlGaN/GaN HEMT sensor based on a microsieve.

2. Materials and methods

2.1 Reagents and chemicals

The zinc acetate ($C_4H_6O_4Zn \cdot 2H_2O$), sodium hydroxide (NaOH), zinc nitrate ($Zn(NO_3)_2$), and hexamethylenetetramine (HMTA) utilized for synthesizing zinc oxide nanorods (NRs) were procured from Aladdin, a Shanghai-based supplier. Ethanolamine (EA) and glutaraldehyde (GA) were obtained from Sinopharm Chemical Reagent Co., LTD. Bovine serum albumin (BSA), urea, glucose, and phosphate-buffered saline solution with a pH range of 7.2–7.4 were also sourced from Aladdin in Shanghai, China. Urease was acquired from McLean located in Shanghai, China. Artificial saliva with a pH range of 6.6–7.1 was obtained from Shanghai Yuanye Biotechnology Co., LTD. Microsphere powder with particle sizes ranging between 3 and 5 μm was purchased from Xiamen Yongchengxin Plastic Co., LTD while the microporous membrane with a pore size of 0.45 μm was sourced from Changde Beekman Biotechnology Co., LTD. The deionized water used throughout this study underwent purification using the Milli-Q water purification method to ensure its quality and purity remained consistently high during the conducted experiments.

2.2 The microfabrication of disposable gate-AlGaN/GaN high electron mobility transistor (HEMT)

The urea sensor with a disposable gate-AlGaN/GaN HEMT structure consists of two components. The heterojunction chip is utilized for the fabrication of the AlGaN/GaN HEMT chips, where a sapphire substrate is employed to grow the buffer layer (1.5 μm gallium nitride), barrier layer (18 nm AlGaN), and cap layer (1.5 nm gallium nitride). To achieve mesa separation, the Cl_2/BCl_3 inductively coupled plasma (ICP) etching technique is employed. A mixed alloy layer of Ti/Al/Ni/Au is then deposited on a 100 μm surface and subjected to rapid thermal annealing at 880 °C for 45 s in an N_2 environment to form ohmic contact. Electrode layers (Ti/Ni/Au) are evaporated using an overlapping deposition method. The gate contact electrode (Ti/Ni/Au) for HEMT devices is prepared through the sputtering technique. Fig. 2 illustrates the preparation diagram of the AlGaN/GaN HEMT structure. On a SiO_2/Si wafer, the disposable chip for

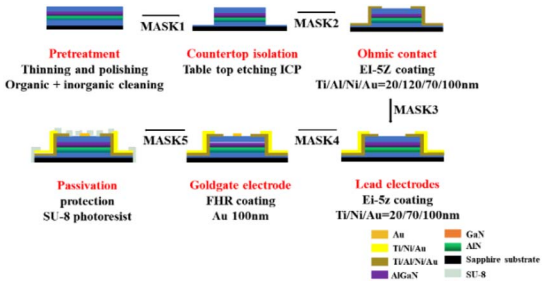

Fig. 2 Fabrication process of the AlGaN/GaN HEMT sensor.

sensing purposes is prepared by depositing a multilayer film of Ti/Au using the sputtering method with a thickness of 120 nm. After the growth of zinc oxide nanorods, the disposable gate chip is connected with the AlGaN/GaN HEMT chip by gold wire.

2.3 Preparation and modification of zinc oxide nanorods by disposable gate chips

The two-step hydrothermal method was utilized for the synthesis of zinc oxide nanorods (ZnO NRs) on a disposable gate chip. To prepare the seed solution, NaOH (0.03 mol) and $C_4H_6O_4Zn\cdot 2H_2O$ (0.01 mol) were dissolved in anhydrous ethanol, followed by refluxing and magnetic stirring at 500 rpm for 2 hours under a water bath temperature of 60 °C. The resulting transparent and clear zinc oxide seed solution was applied onto the clean surface of the disposable gate chip after ultraviolet ozone treatment for 30 minutes. Subsequently, the inoculated chips are vacuum-dried and annealed at 150 °C for 30 min. For growth, a mixture of $Zn(NO_3)_2$ (0.1 mol), HMTA (0.1 mol) and deionized water is stirred until completely mixed to obtain a growth solution. The disposable gate chip is then inverted and suspended in this solution for 3 hours at a temperature of 95 °C to facilitate contact with the growth medium. After the growth process is completed, the surface impurities are removed by rinsing with deionized water, and milky white films (ZnO NRs) are attached to the observation surface. Finally, annealing at 80 °C for an additional 30 min allowed further growth of ZnO NR viscosity in the disposable gate region, as confirmed by electron microscopy analysis shown in Fig. 3.

The bioreceptor on the surface of the disposable gate chip coated with NRs underwent modification enabling detection of target analytes. To improve hydrolysis stability, it received a thorough cleaning and oxidation treatment through exposure to ultraviolet ozone for thirty minutes. Following this step, it was soaked in deionized water for twelve hours prior to immersion in an EA-containing solution for twenty-four hours. Subsequently, sequential washing with ethanol and deionized water effectively removed any residual ethanolamine that remained unbound after which drying occurred utilizing N_2 gas. Next, glutaraldehyde (at a concentration of 1.25%) is used as a powerful fixative and activator to crosslink disposable gate chips for 3 h at room temperature. After rinsing with deionized water, urease (0.1 mmol) is combined to the chip for 12 h at 4 °C. Finally, the chip is immersed in 1% BSA solution to block any non-specific binding caused by the unmodified urease molecular chain. Fig. 4a illustrates the entire process visually, and Fig. 4b shows the *I–V* diagram before and after the device modification. After these modification steps are completed, the disposable gate chip and HEMT chip are routed and packaged to fabricate the urea biosensor.

2.4 Operation mechanism of disposable gate AlGaN/GaN HEMT urea sensor

Because AlGaN/GaN HEMTs are particularly sensitive to changes in surface potential, even small charge shifts in the gate region can produce carrier coupling in the channel, resulting in a change in source drain current (I_{ds}) at a fixed V_{ds}, as shown in the following equation:[49]

$$I_{ds} = \frac{\varepsilon_{AlGaN}\mu_{2DEG}W}{Ld}\left[(V_G - V_T)V_{ds} - \frac{{V_{ds}}^2}{2}\right]$$

where ε_{AlGaN} represents the AlGaN dielectric constant, μ is the electron mobility of 2DEG, V_G is the gate voltage generated by surface conditions, V_T is the threshold voltage, W and L are the channel width and length, respectively, and d represents the total distance between the biological reaction charge center and the 2DEG channel.[38] The equation shows that the variation of I_{ds} of the disposable gate AlGaN/GaN HEMT is related to the variation of the surface potential of the disposable gate.

$$CO(NH_2)_2 + 3H_2O \xrightarrow{\text{urease}} 2NH_4^+ + HCO_3^- + OH^-$$

In this study, detection is achieved by introducing a urea solution into the sensing region of an AlGaN/GaN HEMT disposable gate chip, the experimental detection device of the disposable gate AlGaN/GaN HEMT sensor based on a microsieve has been shown in Fig. 5. Upon enzymatic reaction between uncharged urea and urease occurs, the resulting reaction

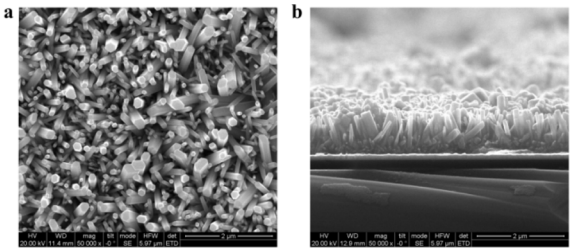

Fig. 3 Growth of zinc oxide nanorod arrays on a disposable grid gold film in field emission scanning electron microscopy (FESEM) images, (a) top view and (b) front view.

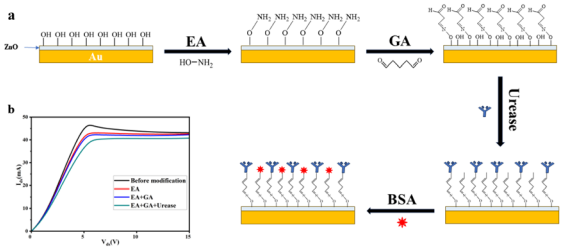

Fig. 4 (a) Biofunctionalization of disposable gate electrodes. (b) Changes in output characteristic curves before and after sensor biofunctionalization.

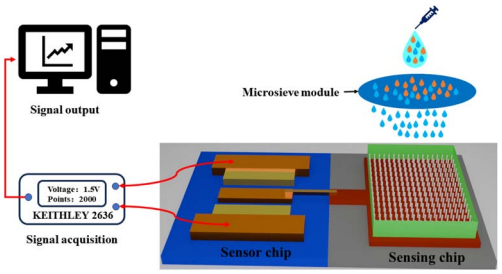

Fig. 5 Experimental detection device of disposable gate AlGaN/GaN HEMT sensor based on a microsieve.

follows the aforementioned process.[42] The presence of EA on the sensing film protects ZnO from corrosion, while the hydroxyl group (–OH) on the surface of ZnO reacts with analyte, which would modify its surface potential and enhance positive charge. As a result, there is an increase in 2DEG concentration, leading to a corresponding rise in I_{ds} at a fixed source under constant V_{ds}.

3. Results and discussion

3.1 Performance of AlGaN/GaN HEMT urea sensors in 0.1× PBS buffer

The urea concentration tested was 1 fM to 100 mM and dissolved with 0.1× PBS. Measurements were started with 0.1× PBS as the baseline. Using the designed sensor, urea is detected in real time at $V_{ds} = 1.5$ V, as shown in Fig. 6a. After adding a target solution containing 1 fM urea to the sensor using a transfer fluid gun, a sudden peak is observed (mechanical interference caused by the use of a transfer fluid gun dynamic addition, as this interference can cause a change in the ionic state in the solution and appears as a peak), followed by a rapid drop in the current within 30 seconds. However, the current does not return to the baseline but maintains a steady value above the baseline. This is because there is a sensing device on the disposable grid for urease to react with urea, resulting in a significant rise in the I_{ds} current (Fig. 6a). The current response for real-time urea measurements is extracted as leakage current from the baseline, $\Delta I = I_{ds,urea} - I_{ds,0.1\times\ PBS}$, $I_{ds,urea}$ for each order of magnitude of the current change caused by urea concentration. As shown in Fig. 6b, it has good linearity ($R^2 = 0.9977$) and excellent sensitivity (6.552 μA dec^{-1}) in the range of 1 fM to 100 mM. As expected, the current gradually rose as the urea concentration increased. In addition, to verify that this current response signal was caused by an enzymatic reaction between urea and urease, a pipette gun was used to continuously add 10× PBS, 10 mM glucose, and 10 mM cortisol to the sensor sensing area, and a sudden peak current was observed, followed by a rapid decline to the baseline level within 30 seconds. When 1 mM urea solution was added, the I_{ds} value showed a significant increase, which verified the current response sensing of specific reactions on the disposable gate.

3.2 Urea determination in artificial saliva by AlGaN/GaN HEMT biosensors with or without the microsieve module

In our work, we put the microsieve module into FESEM (Fig. 7), observed the morphology and pore distribution of the microsieve

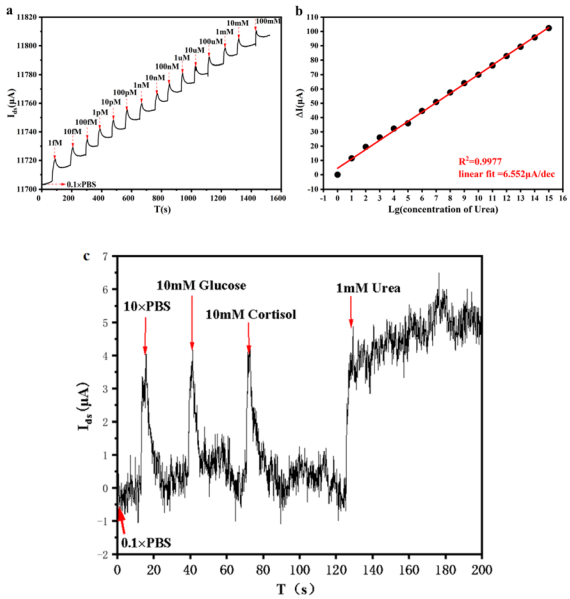

Fig. 6 (a) Relationship between I_{ds} of urea from 1 fM to 100 mM in 0.1× PBS solution and time. (b) Calibration curves of I_{ds} and different urea concentrations. (c) Verification of the specific response of urea signal from urease-modified disposable gate AlGaN/GaN HEMT sensors.

module, and checked whether the aperture of the microsieve module used can achieve the role of screening macromolecular impurities (3–5 μm). Using an electron microscope of 5 μm (Fig. 7a), it could be found that the pore size of the microsieve module is mainly 0.5–1.2 μm, which can block macromolecular impurities to achieve the effect of purifying the physiological solution environment. Fig. 7b shows the morphology of the microsieve module under 10 μm electron microscopy. It can be seen that the pore distribution of the microsieve module is relatively uniform, and the liquid and the small molecule target to be measured can flow normally when the detection solution is added by dripping. The addition of the microsieve module not only cleans the physiological solution environment, but also enables the tested substance to enter the biodetection area of the disposable grid chip smoothly through the microsieve module to complete the subsequent biodetection.

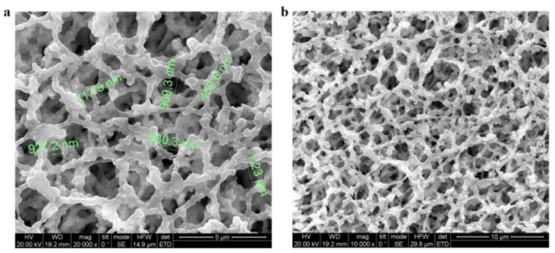

Fig. 7 The growth of a microscreen module on a disposable grid gold film in a field emission scanning electron microscope (FESEM). (a) Using a 5 μm electron microscope, it can be shown that the pore size of the microsieve module ranges from 0.5 μm to 1.2 μm. (b) Using a 10 μm electron microscope, it can be observed that the pore distribution of the microsieve module is uniform.

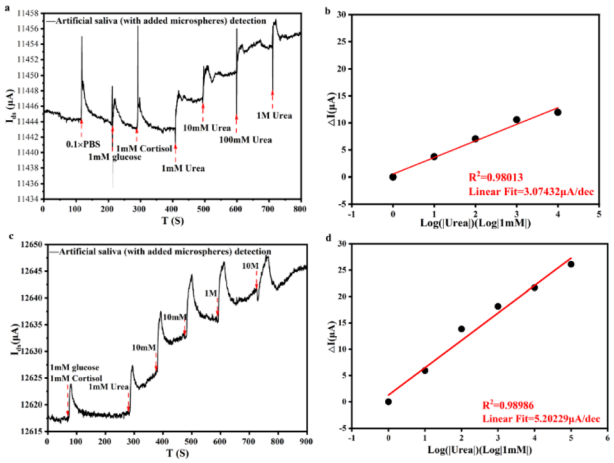

Fig. 8 (a) Detection of I_{ds} curve with urea concentration from 1 mM to 1 M by the sensor without a microsieve. (b) ΔI calibration curve for sensors without a microsieve. (c) The sensor with a microsieve detects the I_{ds} curve with a urea concentration of 1 mM to 10 M. (d) Calibration curve for ΔI of the sensor with a microsieve.

Using a designed sensor, urea was detected under real-time conditions of V_{ds} = 1.5 V, as shown in Fig. 8a. After using a pipette to add 0.1× PBS, 1 mM glucose, and 1 mM cortisol to the sensor, a rapid drop in current was observed within 30 seconds, and then the current returned to the baseline. The introduction of urea solution into I_{ds} showed significant differences. After adding 1 M of urea to the solution to be tested, I_{ds} tended to be saturated and its sensitivity was greatly reduced. The sensitivity of the designed sensor (3.07432 μA dec^{-1}) was significantly reduced when detecting the urea range of 1 mM to 1 M, compared to detection in 0.1× PBS solution (Fig. 8b). This shows that the complex physiological environment will cause interference to the sensor, making the detection results of urea inaccurate.

When we add the microsieve module to the sensing area of the disposable gate AlGaN/GaN HEMT urea sensor, urea detection is performed in artificial saliva, as shown in Fig. 8c. For devices with a microsieve module, the maximum detection limit of urea was increased from 1 M to 10 M before approaching saturation, and the biosensor sensitivity (5.20229 μA dec^{-1}) was significantly improved after the addition of the microsieve module, as shown in Fig. 8d. This shows that the addition of the microsieve module reduces the interference of the microspheres and other impurities in the artificial saliva to the sensor, which greatly improves the performance of the sensor and makes the detection results more real and reliable.

3.3 Bioassay of AlGaN/GaN HEMT biosensors modified with and without the microsieve module in actual saliva

To further confirm that the microsieve module can make HEMT sensors more accurate in real saliva solutions, we compared the detection of urea current signal changes in saliva with and without the microsieve sensor, as shown in Fig. 9. As shown in Fig. 9a and b, when human saliva solution was added to the sensor without the microsieve module, the current signal did

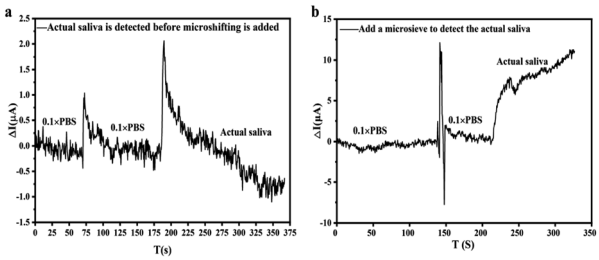

Fig. 9 Urea determination using AlGaN/GaN HEMT biosensors in human saliva. (a) No microsieve HEMT sensor. (b) Microsieve HEMT sensor.

not show a significant increase but a decrease, indicating that our device could not detect accurate and reliable urea sensing data in saliva. When we added human saliva solution to the sensing area of the sensor with the microsieve module, the current signal showed a significant increase in response, ΔI of about 5 μA, which is consistent with the sensitivity data detected in artificial saliva. It was confirmed that the AlGaN/GaN HEMT biosensor without the microsieve module could not directly detect urea in human saliva or could cause inaccurate detection. The AlGaN/GaN HEMT biosensor based on the microsieve module can screen impurities and reduce environmental interference, so that the urea response current is basically not affected, making urea detection and detection results more accurate. Therefore, the AlGaN/GaN HEMT biosensor based on the microsieve module can achieve the application requirements of direct detection of urea in the human saliva environment.

4. Conclusion

In conclusion, we present the study of a disposable gate AlGaN/GaN HEMT biosensor based on a microsieve module for the detection of urea content in saliva. The addition of the microsieve structure enhanced the detection sensitivity of the sensor in artificial saliva (5.20229 μA dec^{-1}) to achieve a high detection limit (10 Mmol). In addition, our designed disposable gate HEMT sensor has a high sensitivity of about 6.552 μA dec^{-1} for urea from 1 fM to 100 mM in 0.1× PBS solution, which correlates with actual salivary urea analysis. Compared to current urea biosensors, our optimized sensor shows a wider linear range and lower detection limits. Our disposable gate AlGaN/GaN HEMT biosensor based on a microsieve module is much simpler than today's centrifuge and expensive laboratory equipment. The AlGaN/GaN HEMT biosensor cannot be used to detect analytes in physiological solution.

Conflicts of interest

There are no conflicts to declare.

Acknowledgements

This work was supported in part by the program of NSFC under project 62074159 and in part by the State Key Laboratory of

Precision Measuring Technology and Instruments (Tianjin University) under Grant pilab 2212. The authors also acknowledge the Nano-Characterization and Nano-Fabrication Platforms at the Suzhou Institute of Nano-Tech and Nano-Bionics, Chinese Academy of Sciences, for their supports of fabrication and characterization.

References

1 J. Kim, A. S. Campbell, B. E. de Ávila and J. Wang, *Nat. Biotechnol.*, 2019, **37**, 389–406.
2 A.-H. Farzaneh, D. I. Mirzaii and A. Sara, *J. Contemp. Dent. Pract.*, 2006, **7**, 104–111.
3 H. Mese and R. Matsuo, *J. Oral Rehabil.*, 2007, **34**, 711–723.
4 J. P. Chandhana, P. Navaneeth, V. S. Punathil, P. Aarathi, B. G. Nair and B. T. G. Satheesh, *Microchim. Acta*, 2023, **190**, 390.
5 Z. Liu, Y. Chen, M. Zhang, T. Sun, K. Li, S. Han and H. J. Chen, *Biosensors*, 2021, **11**, 242.
6 E. M. O'Sullivan, D. Paul, S. Dieter and O. Kay, *Methods Mol. Biol.*, 2023, **2596**, 147–167.
7 L. V. Bel'skaya, E. A. Sarf and V. K. Kosenok, *Klin. Lab. Diagn.*, 2018, **63**, 477–482.
8 R. Venkatapathy, V. Govindarajan, N. Oza, S. Parameswaran, B. Pennagaram Dhanasekaran and K. V. Prashad, *Int. J. Nephrol.*, 2014, **2014**, 742724.
9 B. N. V. S. Satish, P. Srikala, B. Maharudrappa, M. A. Sharanabasappa, K. Prashant and H. Deepa, *J. Int. Oral Health*, 2014, **6**, 114–117.
10 K. H. Wang, J. C. Hsieh, C. C. Chen, H. W. Zan, H. F. Meng, S. Y. Kuo and M. T. N. Nguyen, *Biosens. Bioelectron.*, 2019, **132**, 352–359.
11 P. Divya, N. A. Kumar and K. S. Ravi, *J. Clin. Diagn. Res.*, 2016, **10**, ZC58–ZC62.
12 S. S. Low, Y. Pan, D. Ji, Y. Li, Y. Lu, Y. He, Q. Chen and Q. Liu, *Sens. Actuators, B*, 2020, **308**, 127718.
13 A. N. M. Kelkar, *Abstr. Pap. Am. Chem. Soc.*, 2020, **248**, 16–22.
14 G. Tansu, K. Volkan and S. Mustafa, *Anal. Sci.*, 2020, **37**, 561–567.
15 L. G. Shaidarova, I. A. Chelnokova, I. A. Gafiatova, A. V. Gedmina and H. C. Budnikov, *J. Anal. Chem.*, 2023, **78**, 372–377.
16 Z. R. J. X, K. Peggy, O. K. L, L. Manuel and H. Shu-Gui, *Biochem. Cell Biol.*, 2009, **87**, 541–544.
17 H. N. Haugen and E. M. Blegen, *Scand. J. Clin. Lab. Invest.*, 2009, **5**, 63–66.
18 V. V. Afanas'ev, T. P. Vavilova, M. V. Osokin and A. V. Pushkin, *Stomatologiia*, 2006, **85**, 29–31.
19 S. Akduman, *F1000Research*, 2019, **8**, 388.
20 G. Mohan, H. Lin, H. Tianyang, P. Anju, Z. Xiaozhuo, D. Haiyun and G. Shuliang, *J. Clin. Med.*, 2022, **11**, 6709.
21 G. Hengxing, W. Jing, Z. Xuexue, Z. Kun, Z. Jiejun and C. Mingwei, *Exp. Gerontol.*, 2022, **169**, 111960.
22 M. Emokpae, H. Osadolor, T. Dagogo and L. Emokpae, *J. Med. Biomed. Res.*, 2013, **12**, 225–233.
23 P. H. Joon, W. S. Hee, K. D. Hee, S. S. Hwan, L. J. Young, L. W. Jeong, H. Sungyoup, C. Kyungman, Y. C. Song and P. Sanghyun, *J. Infect. Chemother.*, 2020, **27**, 387–389.
24 Y. Xie, B. Bowe, T. Li, H. Xian, Y. Yan and Z. Al-Aly, *Kidney Int.*, 2018, **93**, 741–752.
25 B. J. A. Martins, d. S. V. E. Everton, S. Landulfo and F. A. Barrinha, *J. Biomed. Opt.*, 2016, **21**, 59801.
26 S. Yandi, L. Jingjia, Q. Zihao, Y. Ze, J. Xueyao, L. Yindan, H. Qian, Z. Lihong and L. Yan, *Genes*, 2021, **12**, 498.
27 J. A. Martins Bispo, E. E. de Sousa Vieira, L. Silveira Jr and A. B. Fernandes, *J. Biomed. Opt.*, 2016, **21**, 087004.
28 L. Cheng, W. Zheng, Y.-N. Zhang, X. Li and Y. Zhao, *IEEE Trans. Instrum. Meas.*, 2023, **72**, 1–7.
29 B. Alev-Tuzuner, A. Beyler-Cigil, M. V. Kahraman and A. Yarat, *Int. J. Polym. Mater. Polym. Biomater.*, 2019, **68**, 597–606.
30 J.-W. Kang and W.-J. Cho, *Solid-State Electron.*, 2018, **152**, 29–32.
31 P. Bergveld, *Sens. Actuators, B*, 2003, **88**, 1–20.
32 T. M. I. Bin, K. Mohit, H. Yacine, L. Mathieu, S. N. Yves, B. Karim, M. Tarik, N. T. Huong, B. Hafsa, O. Safa, R. Aurelien, G. Thomas, P. Jacques and G. Simon, *Int. J. Hydrogen Energy*, 2024, **55**, 1514–1522.
33 K. Wang, Y. Zhu, H. Zhao, R. Zhao and B. Zhu, *Electronics*, 2024, **13**, 363.
34 V. Hemaja and D. K. Panda, *Silicon*, 2021, **14**, 1–14.
35 R. Kirste, N. Rohrbaugh, I. Bryan, Z. Bryan, R. Collazo and A. Ivanisevic, *Annu. Rev. Anal. Chem.*, 2015, **8**, 149–169.
36 T. T. Yu, S. Anirban, S. Indu, P. A. Kumar, W. S. Li, S. S. Chu, L. G. Bin and W. Y. Lin, *Sens. Mater.*, 2018, **30**, 2321.
37 L. Diao, Z. Xu, W. Zhang, B. Miao, Y. Hu, Z. Gu and J. Li, *Electroanalysis*, 2022, **34**, 1372–1380.
38 Z. Gu, J. Wang, B. Miao, X. Liu, L. Zhao, H. Peng, D. Wu and J. Li, *IEEE Sens. J.*, 2021, **21**, 2552–2558.
39 S. Yang, L. Gu, X. Ding, B. Miao, Z. Gu, L. Yang, J. Li and D. Wu, *IEEE Electron Device Lett.*, 2018, 1.
40 X. Ding, S. Yang, B. Miao, L. Gu, Z. Gu, J. Zhang, B. Wu, H. Wang, D. Wu and J. Li, *Analyst*, 2018, **143**, 2784–2789.
41 L. Gu, S. Yang, B. Miao, Z. Gu, J. Wang, W. Sun, D. Wu and J. Li, *Analyst*, 2019, **144**, 663–668.
42 J. Wang, Z. Gu, X. Liu, L. Zhao, H. Peng and J. Li, *Analyst*, 2020, **145**, 2725–2730.
43 X. Liu, L. Zhao, B. Miao, Z. Gu, J. Wang, H. Peng, J. Li, W. Sun and J. Li, *Electroanalysis*, 2019, **32**, 422–428.
44 J. Wang, Z. Gu, B. Miao, L. Zhao, X. Liu, J. Cheng, Z. Zhang and J. Li, *Electroanalysis*, 2019, **31**, 2404–2409.
45 Z. Gu, J. Wang, B. Miao, L. Zhao, X. Liu, D. Wu and J. Li, *RSC Adv.*, 2019, **9**, 15341–15349.
46 L. Zhao, X. Liu, B. Miao, Z. Gu, J. Wang, H. Peng, J. Zhang, B. Zeng and J. Li, *Anal. Methods*, 2019, **11**, 3981–3986.
47 M. Park, R. Thapa and A. Son, *Meeting Abstracts*, 2017, vol. MA2017-02, p. 2339.
48 Y. W. Chen, C.-P. Hsu, I. Sarangadharan and Y.-L. Wang, *ECS Trans.*, 2017, **77**, 21–25.
49 J.-d. Li, J.-j. Cheng, B. Miao, X.-w. Wei, J. Xie, J.-c. Zhang, Z.-q. Zhang, H.-W. Li and D.-m. Wu, *Microsyst. Technol.*, 2014, **21**, 1489–1494.

